



Characterization of the deterioration of externally bonded CFRP-concrete composites using quantitative infrared thermography

W.L. Lai^a, S.C. Kou^a, C.S. Poon^{a,*}, W.F. Tsang^b, C.C. Lai^b

^a Department of Civil and Structural Engineering, The Hong Kong Polytechnic University, Hong Kong

^b Department of Building and Real Estate, The Hong Kong Polytechnic University, Hong Kong

ARTICLE INFO

Article history:

Received 7 May 2008

Received in revised form 18 March 2010

Accepted 20 March 2010

Available online 27 March 2010

Keywords:

Interfacial flaws

Interfacial delamination

CFRP-concrete composite

Quantitative infrared thermography

Deterioration

ABSTRACT

Defects embedded in externally-bonded CFRP-concrete composite structures reduce the interfacial bond strength and durability. This paper classifies these defects into two types: flaws and delaminations. Flaws are formed during the first application of the CFRP strips onto the concrete surface due to poor workmanship. Delaminations are formed due to stress concentrations related to chemical/physical degradation of the binding layer. In this study, an aggressive environment was simulated by placing the specimens in water baths with elevated temperatures (40 °C and 60 °C). The sizes of the CFRP-flaws and delaminations were determined by (i) quantitative infrared thermography (QIRT) and (ii) processing of visual images after opening-up the CFRP by direct shear. Experimental results show that apparent flaw sizes determined by QIRT were in good agreement (88% accuracy) with actual flaw sizes determined by the image processing method. The results also show that flaws exhibited little change but the bonding layer showed significant deterioration after exposure to high water temperatures.

© 2010 Elsevier Ltd. All rights reserved.

1. Introduction

This paper presents a method to define the boundaries and estimate quantitatively the sizes of flaws and delaminations within the externally bonded CFRP-concrete interfaces. These unseen defects embedded in the interface between the CFRP and concrete elements can significantly reduce the effective contact area and therefore the overall bond strength. Ultimately the durability and the service life of a CFRP strengthened concrete structure (such as a highway bridge) would be adversely affected.

The quality of interfacial bond varies according to the properties of materials and workmanship when the adhesive bonding (e.g. epoxy resin) system is applied. As a result, the occurrence of voids or flaws is quite common. Another type of bonding defect found in the interfacial bond is interfacial delaminations (or simply delaminations) developed due to the deterioration of bonding layer (epoxy resin) of the CFRP-concrete composites when the composite is exposed to aggressive environments such as elevated temperatures, ultraviolet radiation, infiltration of moisture and extreme temperatures caused by fire. When these degrading processes occur, chemical/physical changes of the epoxy resin deteriorate the effective bond quality and hence the bond strength is reduced.

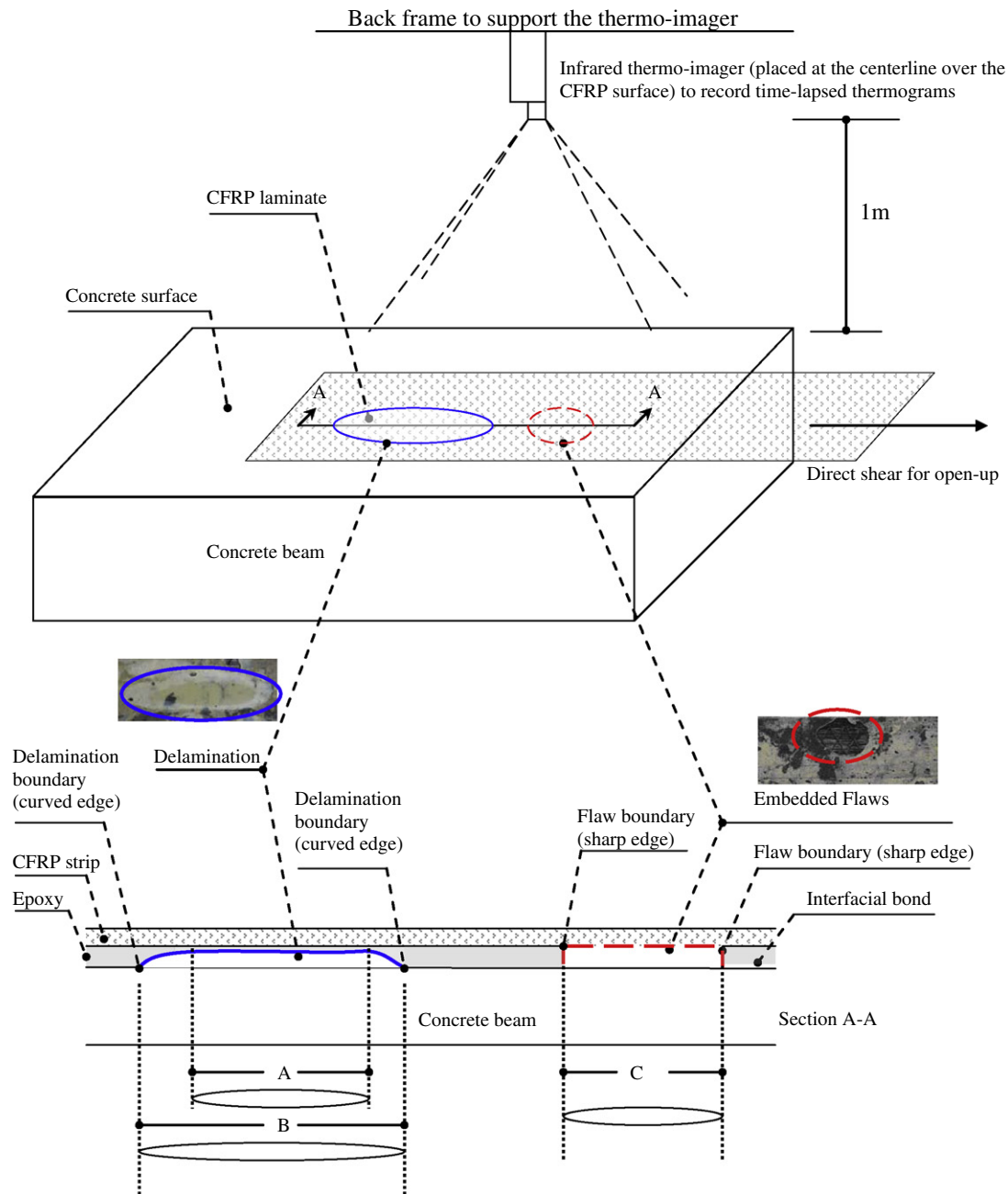
Conventional methods of evaluating the bond quality of the CFRP-concrete composites are hammer-tapping and pull-off tests.

* Corresponding author.

E-mail address: cecspon@polyu.edu.hk (C.S. Poon).

Hammer-tapping requires manual point contact by the inspection personnel; and the pull-off test is destructive. Both type of tests are regarded as localized tests and do not allow effective and large-scale inspection. Infrared thermographic (IRT) technique has been widely accepted as an effective means to identify and quantify unseen surface flaws in a wide range of composite materials. Some of the recent applications include assessing materials such as aluminium corrosion [1], glass-epoxy laminates [2], plastic lids [3], externally bonded CFRP-concrete composites [4–7] and concrete voids up to 10 cm deep [8,9]. In these various applications, the embedded flaws are not readily noticed by the naked eyes, but can be detected non-destructively, remotely and effectively by using non-contact IRT. It is because the presence of a defect (i.e. air layer) in a composite/homogeneous material reduces the heat diffusion rate once a thermal stimulus is applied. Fundamental principles of using IRT to solve a variety of civil engineering and nondestructive testing problems are well documented in [10–12], whilst an excellent review of recent IRT applications is given by [13]. During the early application of IRT, most published works focused simply on locating the embedded flaws qualitatively, while it is more necessary to quantify the flaw sizes so that the extent of damages can be assessed.

Quantitative characterization of defects using infrared data can be achieved based on direct analytical methods [10,14] and inverse methods [10,15]. The direct analytical approaches can be used to model the defect characteristics but this approach can be very complex even when the defect geometries are simple, and may degenerate into unworkable situations when anisotropic



Note: Widths B and C are defined as the boundaries of delamination and flaw in this paper respectively

Fig. 1. Embedded delaminations and flaws contained within a CFRP-strengthened concrete prism.

properties and subsurface defects are considered [10]. Therefore in this paper, a relatively simple inverse method, known as two-inflection point algorithm, is presented to define the defect boundaries and provide estimates of the defect areas within the CFRP-concrete interfaces. This method, along with quantitative infrared thermography (QIRT), are jointly adopted for analysis of the thermo-signals and defect characterization.

2. Experimental setup

2.1. Materials and specimens

The CFRP strips (sized 60×200 mm and 0.165 mm thick) and the concrete prisms (sized $150 \times 150 \times 350$ mm) were bonded

Table 1

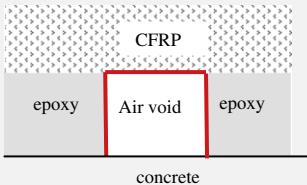
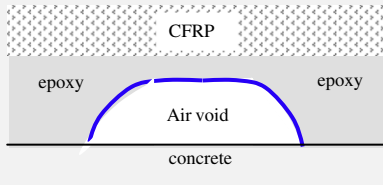
Tensile properties of CFRP and epoxy resin.

Type of specimen	Number of specimens tested	Elastic modulus (MPa)	Elongation (%)	Tensile strength (MPa)
25 mm wide CFRP strip	5	254,860	1.482	4163
25 mm wide Sika 300 coupon	5	26,354	1.212	86

using a proprietary epoxy resin system (Sika 300™), as shown in Fig. 1. A number of physical properties of the CFRP strips and Sika 300™ were determined according to the flat coupon tensile tests

Table 2

Definitions, illustrations and methods to quantify flaws and delaminations.

Types of bond defect	A flaw	A delamination
Illustration of defect cross-section		
Appearance after open-up	Black color, imperfect circular shape and sharp edge	Grey color, elliptical or irregular shape and curved edge
Methods to quantify defect boundaries and areas		
Before exposure	QIRT and two-inflection point algorithm	
After exposure	QIRT and two-inflection point algorithm and digital image analysis	Digital image analysis

[16,17] and the test results are reported in Table 1. The mix proportions of the concrete prisms were (1) (OPC ASTM Type I cement) (2) (river sand) (3) (10 mm and 20 mm natural crushed granite) with a water/cement ratio of 0.50 and the average 28 day cube compressive strength was 39 MPa. The Sika 300 was mixed by weight in a ratio of 3-part epoxy to one-part hardener. The epoxy and hardener

were mixed for at least 5 min using an electric mixer until the mixture appeared uniform.

2.2. Interfacial bond between CFRP strips and concrete

The concrete surface was roughened using a mechanical grinder to remove all surface laitance and expose the coarse aggregates. Dust from the concrete surface was then removed using a high power vacuum cleaner. To maintain the thickness of the epoxy resin to about 1.5 mm, 1.5 mm thick aluminium spacers were adhered on the concrete surface prior to laying the binder. The prepared epoxy resin was applied onto the concrete and CFRP strip surfaces at the same time, and CFRP strips were laid in position by applying dead weights. After laying the CFRP strips on the concrete prisms, the fresh epoxy resin was allowed to harden for at least 14 days before QIRT tests were conducted.

Two types of defects were classified in the interfacial bond, namely (i) sharply-edged flaws and (ii) curved-edge delaminations (see Table 2 and Fig. 1). The sharply-edged flaws were entrapped air voids formed during the initial application of the CFRP strips to the concrete surface due to poor workmanship such that the interlayer epoxy resin was not able to completely fill up the entire interface between the CFRP and concrete. The delaminations, on the other hand, were formed due to stress concentration as a result of chemical/physical degradation of the binding layer (i.e. epoxy resin) when the composite was exposed to aggressive environments.

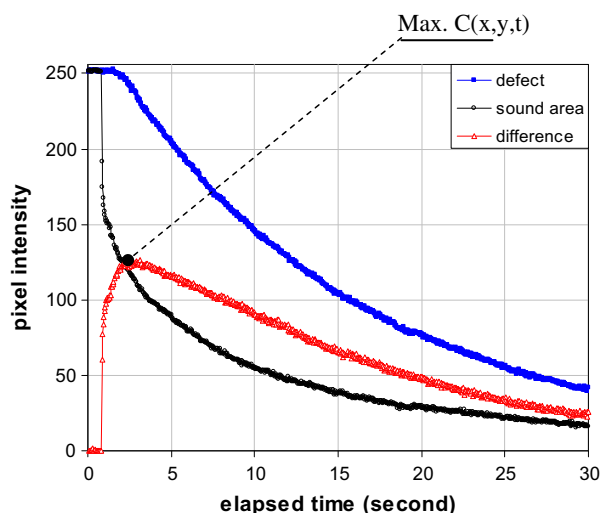


Fig. 2. Thermal history curves of the flaw and sound areas.

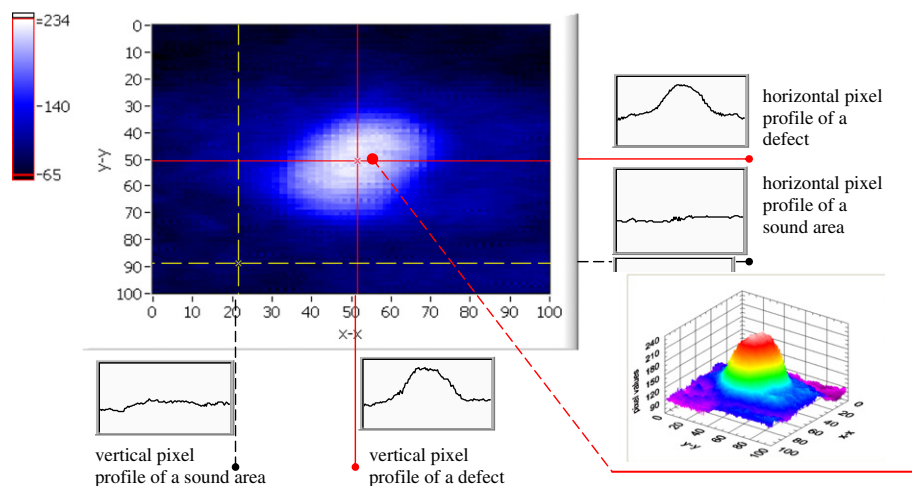


Fig. 3. Thermogram of a flaw and respective pixel profiles.

2.3. Exposure conditions

The specimens in three batches were put into three separate fresh water chambers maintained at 25 °C, 40 °C and 60 °C respectively. These exposure conditions were maintained for 50 weeks.

3. Testing methods

3.1. Quantitative infrared thermography (QIRT)

3.1.1. Instrumentation

The infrared thermo-imager used in the experiments was a FLIR Prism DS IR thermo-imager with spectral range 3.6–5 μm. Since digital interfaces were not available, gray-scale video images in analog format were output to a PC via a video output, and through a shielded and short (1 m long) coaxial cable to reduce signal degradation. These analog video images were then encoded to a sequence of 8-bit digitized and two-dimensional thermograms/pixel arrays through an A/D process. The A/D process was controlled via the National Instrument hardware and an in-house software program developed under the LabVIEW™ and IMAQ™ environment. In each experiment, the software program was designed to capture and process the thermograms frequently (sampling rate = 25 frames per second) and continuously (for 30 s) so that the transient differences of heat transfer could be closely monitored. For each of the experiment lasting for 30 s, 750 frames were captured.

The 8-bit digitized thermograms contained pixel values ranging from 0–255. This range was assumed to represent linearly the temperature values ranging from the lower bound to the upper bound. The temperature scale was annotated in each thermogram. The lower bound was 22 °C which was approximately the room temperature; whereas the upper bound was 40 °C which was approximately the controlled heated temperature. Temperature accuracy was thus equal to $(40-22)/256 = 0.07\text{ °C} \approx 0.1\text{ °C}$.

The thermal stimulus used in the experiments was a hot pack with a fairly constant surface temperature (40 °C). For each test run, it was applied directly on the CFRP surface for 30 s to supply evenly distributed heat energy on the specimens so that the defective and the sound areas in the interfacial bond can be distinguished and characterized through different heat diffusion rates.

3.1.2. Maximum thermal contrast

The thermal events occur within a defect or a sound area change with time (Fig. 2) because heat dissipation is time-dependent. Thus selection of an appropriate and fixed thermogram at a particular instant is required to extract and define the local flaw boundaries. The selection criteria is generally based on the thermogram with the greatest thermal contrast [10] which is the temperature differential of the flaws normalized over a sound area, as shown in Eq. (1) and Fig. 2. This equation combines the temporal (i.e. t) and the spatial (i.e. x and y) references of the thermal contrast [19,20].

$$C(x, y, t) = \frac{\Delta T_{\text{def}}(x, y, t)}{\Delta T_{\text{sound}}(x, y, t)} = \frac{T_{\text{def}}(x, y, t) - T_{\text{def}}(t_0)}{T_{\text{sound}}(t) - T_{\text{sound}}(t_0)} \quad (1)$$

where $C(x, y, t)$ is the spatial thermal contrast at any time t ; $T_{\text{def}}(x, y, t)$ is the spatial temperature (represented by pixel values) at which the defects are found at any time t ; $T_{\text{def}}(t_0)$ is the spatial temperature (represented by pixel values) at which the defects are found initially; $T_{\text{sound}}(t)$ is the temperature (represented by pixel values) at a particular position at which no defects are found at any time t ; $T_{\text{sound}}(t_0)$ is the temperature (represented by pixel values) at a particular position at which no defects are found initially; and

$T_{\text{def}}(t_0) = T_{\text{sound}}(t_0)$ if the defective and sound areas in the specimen were assumed to attain the same temperature.

3.1.3. Two-inflection point algorithm for defining flaw boundaries

After the extraction of the appropriate thermogram at Max $C(x, y, t)$ as shown in Fig. 2, the thermogram was digitized and the associated geometrical shape of the defect was estimated by the apparent shape deduced from the pixel profile shown in Fig. 3. The latter was found to be close to the steepest temperature gradient computed on the sample surfaces over the defects [15], which is known as gradient computation method [10]. Such method may be processed with a number of algorithms, such as Roberts gradient [18], high degree approximation [10], second order fit [10] and inflection point [4,6]. In this paper, the inflection point algorithm was adopted and modified as two-inflection point algorithm as follows.

The column (in y - y direction) and row (in x - x direction) pixel slices related to the thermogram of each of the flaw were extracted, as depicted in Fig. 3. Each of these column and row pixel profiles was segmented at about the mid-point (i.e. center of the flaw) to construct two sub-pixel profiles; which were then curve-fitted into the 4th order polynomials $P(x)$, as illustrated in the zone 1 and 2 in Fig. 4. $P(x)$ was subsequently differentiated twice to obtain another 2nd order equation, where one of the respective roots in this equation was the inflection point (w_{boundary}) of $P(x)$, as represented in equation [2].

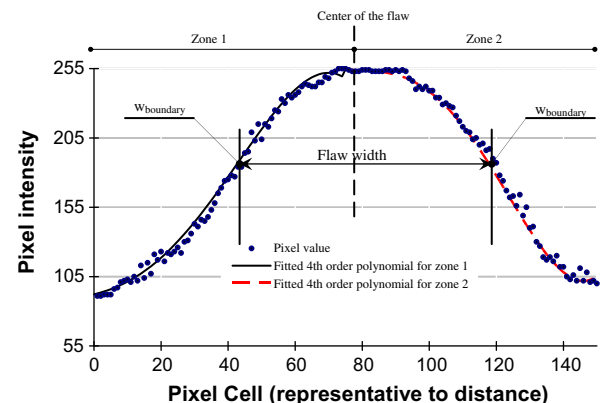
$$\frac{\partial^2 P(x)}{\partial x^2} = 0 \quad \text{at } w_{\text{boundary}} \quad (2)$$

where x = pixel cell; w_{boundary} = the pixel cell defined as flaw boundary; and $P(x)$ = pixel intensity as a function of pixel cell.

The number of pixels from the inflection point to the mid-point in the defect thermogram was then counted. This count represented the apparent half-width of the defects at a particular column or row. Summation of the total apparent half-width gave the apparent sizes of the defects in each row/column sub-pixel profile. For all areas identified to exhibit slow thermal decay that indicates presence of a defect, the aforementioned process was programmed to iterate for each column and row shown in the thermograms.

3.2. Digital image analysis of flaw and delamination boundaries

The sizes of the actual flaws and delaminations found in the CFRP-concrete composite were inspected by opening up the composites by direct shear (see the setup in Fig. 1) and quantified with



Remark: separation of each pixel cell is 0.4mm. Flaw width in this figure = $80 \times 0.4\text{mm} = 32\text{mm}$.

Fig. 4. Pixel profile from a flaw to sound zone.

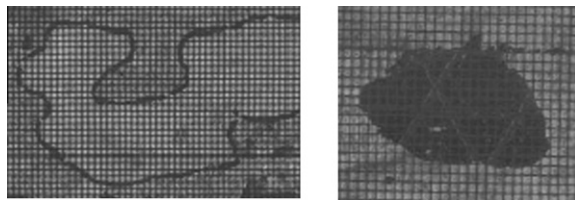


Fig. 5. Interfacial delamination (left) and flaw (right) overlaid by 1 mm² grid for visual imaging method.

the aid of a visual image analysis. For the delaminations, the sizes were determined by: (i) firstly drawing boundaries manually on the CFRP strips (Fig. 5, left); (ii) secondly scanning the CFRP strip overlaid by a transparency printed with 1 mm² grid and converting those in image files; and (iii) finally the defective areas were computed with the aid of a commercially available visual imaging software. For the flaws, the steps used were the same as those for delaminations, except that the first step was omitted because unlike delaminations, the contrast of the flaw boundary was sufficiently clear (as shown in the right side of Fig. 5).

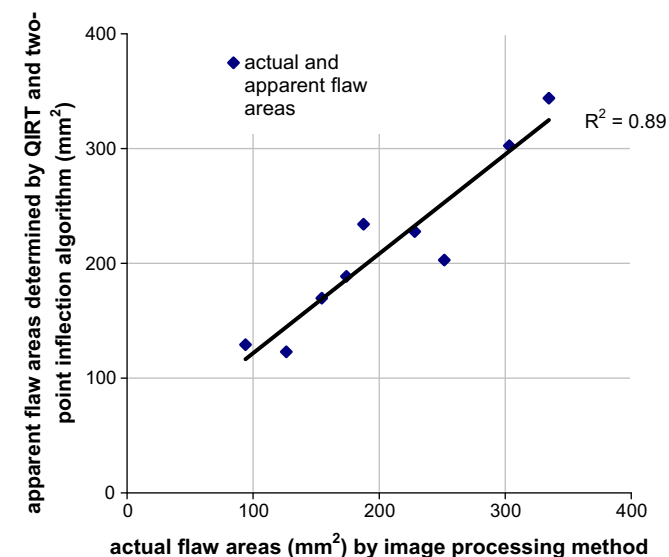


Fig. 6. Comparison between the actual and apparent flaw sizes.

4. Results and discussion

4.1. Correlation of apparent and actual flaw sizes

Fig. 6 compares the apparent (determined by QIRT) and actual (determined by image analysis after opening-up) flaw sizes after exposure. The accuracy is 88% and the correlation coefficient is 0.89. These results validate the appropriateness of QIRT and the two-inflection point algorithm methods for the estimation of size of the defects in the CFRP-concrete composite after the exposure period. This is consistent with the results of our previous study based on 17 artificially implanted flaws in the CFRP-concrete composite [6].

4.2. Effects of elevated temperatures on flaws and delaminations

Fig. 7 illustrates two examples of typical infrared thermograms and opening-up photos of the CFRP-concrete interface captured before and after exposing the specimens to the elevated temperatures, and after open-up with direct shear (Fig. 1). The size of the flaw in example 1 exhibited little changes after exposure. In example 2, the IRT thermogram shows the development from no delamination (before exposure) to a large delamination (after exposure).

The results shown in Fig. 8 illustrate the sizes of the sharp-edged flaws were not affected by the exposure condition. It is probably because these flaws were air voids entrapped during the initial laying of the CFRP on the concrete surface and there is no initiation of swelling stress to extend the flaw boundary in the course of exposure.

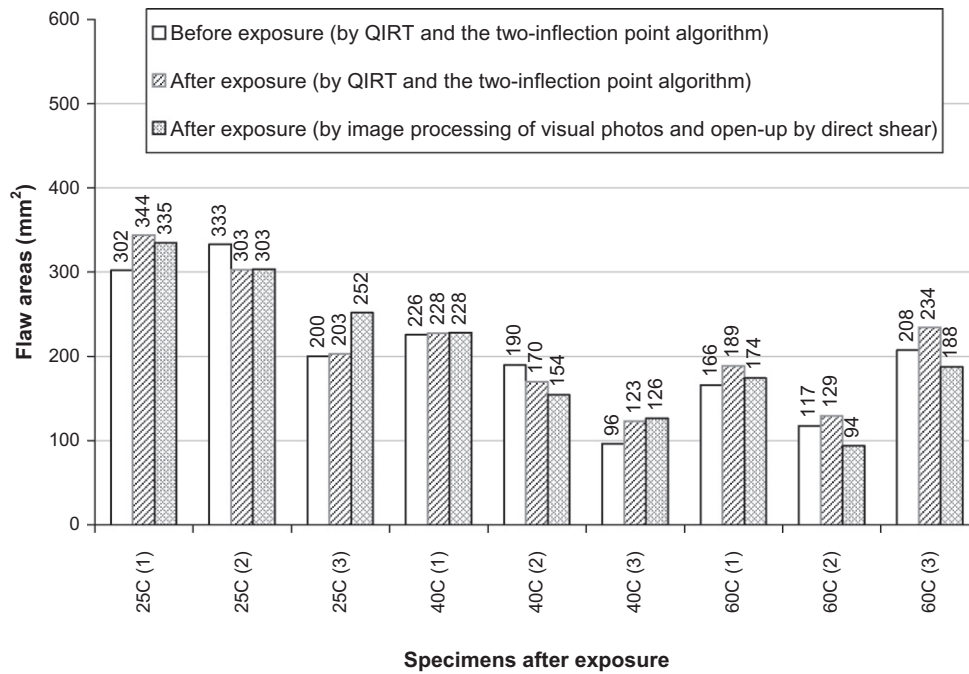
On the contrary, elevated temperatures contributed to significant deterioration of the epoxy resin and led to the development of delaminations as revealed in example 2 of Fig. 7. The delaminations were not present before the exposure. Fig. 9 shows the effect of different exposure water temperatures on the development of the delaminations as revealed by open-up examination. Attempts had been made to define the delamination boundaries using the QIRT and two-point inflection method but the results obtained were not consistent with those obtained from the image processing method after opening-up. Therefore, they are not presented in Fig. 9 and a better algorithm is yet to be developed. The inconsistent results were probably due to the relatively flatter pixel profile (illustrated in Table 2) over the delamination areas, when compared with the sharp-edged pixel profile over the flaw areas, rendering clear demarcation of the delamination areas difficult.

No observable deterioration was noticed for the specimens that were exposed to 25 °C. However, significant deterioration was

Sample type	Thermograms before open-up		Photos after open-up
	Before exposure	After exposure	
Example 1: flaw with little change after exposure	 flaw in thermogram at Max (x,y,t) where elapsed time = 4.6s (area = 226mm ²)	 flaw in thermogram at Max (x,y,t) where elapsed time = 6.2s (area = 228mm ²)	
Example 2: large delamination due to exposure	 no delamination	 delamination 'B' in thermogram at Max C(x,y,t) at elapsed time = 4.7s (area = 2953mm ²)	

Remark: elapsed time refers to the time lapsed after the specimen surface reached the highest temperature.

Fig. 7. Conditions of the sharp-edge flaw and development of delamination due to exposure to elevated water temperature.



Remark: The specimen ID in x-axis indicates the exposure temperatures in °C in the water bath.

Fig. 8. Comparison of flaw areas before and after exposures.

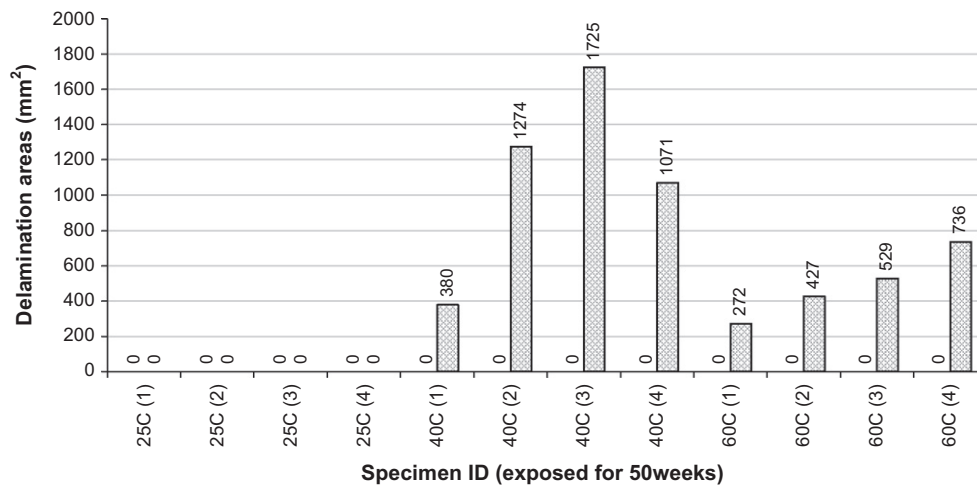


Fig. 9. Comparison of delamination areas after exposures.

observed at exposure temperatures of 40 °C and 60 °C. It is probably because at above a certain critical temperature, water molecules started to act as a resin plasticizer, and the bonds in the polymer (epoxy) chains were disrupted [7,21,22]. The induced swelling stresses may cause permanent polymer matrix cracking, hydrolysis and some degree of fiber-matrix de-bonding [22,23] thus forming the delaminations. The interfacial shear strength would also be reduced [7].

5. Conclusions

In this paper, quantitative infrared thermography (QIRT), together with the two-inflection point algorithm, was developed to analyze the thermo-signals and to relate, characterize and differentiate interfacial flaws embedded and delaminations generated in externally bonded CFRP-concrete composites. In particular, the apparent flaw sizes estimated by QIRT were verified by the image processing method after opening-up the composite to have 88%

accuracy. The effects of exposure to elevated water temperatures on the flaw sizes were also studied. The study results concluded that the original entrapped air voids, or flaws, exhibited little change but the bonding layer (epoxy resin) showed significant deterioration due to the higher water temperatures.

Acknowledgements

The authors would like to acknowledge the funding support of The Hong Kong Polytechnic University and the Research Grants Council (PolyU 5268/08E).

References

- [1] Vallerand S, Maldague X. Defect characterization in pulsed thermography: a statistical method compared with Kohonen and Perceptron neural networks. *NDT&E International* 2000;33:307–15.
- [2] Giorleo G, Meola C. Comparison between pulsed and modulated thermography in glass-epoxy laminates. *NDT&E International* 2002;35:287–92.

- [3] Legrand AC, Meriaudeau F, Gorria P. Active infrared non-destructive testing for glue occlusion detection within plastic lids. *NDT&E International* 2002;35: 177–87.
- [4] Starnes MA, Carino NJ, Kausek EA. Quantitative infrared thermography for quality control of concrete structures strengthened with FRP composites. In: *Proceedings of the American concrete institute 2002 international conference*. Detroit.
- [5] Galietti U, Luprano V, Nenna S, Spagnolo L, Tundo A. Non-destructive defect characterization of concrete structures reinforced by means of FRP. *Infrared Phys Technol* 2007;49:218–23.
- [6] Lai WL, Kou SC, Poon CS, Tsang WF, Ng SP, Hung YY. Characterization of flaws embedded in externally bonded CFRP on concrete beams by infrared thermography and shearography. *J Nondestr Eval* 2008;28:27–35.
- [7] Lai WL, Kou SC, Poon CS, Tsang WF, Lai CC. Effects of elevated water temperatures on interfacial delaminations, failure modes and shear strength in externally-bonded CFRP-concrete beams using infrared thermography, gray-scale images and direct shear test. *Constr Build Mater* 2009;23:3152–60.
- [8] Maierhofer C, Wiggensauser H, Brink A, Röllig M. Quantitative numerical analysis of transient IR-experiments on buildings. *Infrared Phys Technol* 2004;46:173–80.
- [9] Weritz F, Arndt R, Röllig M, Maierhofer C, Wiggensauser H. Investigation of concrete structures with pulse phase thermography. *Mater Struct* 2005;38: 843–9.
- [10] Maldague XPV. *Theory and practice of infrared technology for nondestructive testing*. Wiley-Interscience, John Wiley&Sons, Inc.; 2001.
- [11] Bungey JH. *The testing of concrete in structures*. New York: Surrey University Press; 2006.
- [12] Malhotra, Carino. *Handbook of nondestructive testing of concrete*. Boca Raton: CRC; 2006.
- [13] Meola C, Carlomagno GM. Recent advances in the use of infrared thermography. *Meas Sci Technol* 2004;15:R27–58.
- [14] James PH, Welch CS, Winfree WP. A numerical grid generation scheme for thermal simulation in laminated structures. In: Thompson DO, Chimenti DE, editors. *Review of progress in quantitative nondestructive evaluation*, vol. 8A. New York: Plenum Press; 1989. p. 801–9.
- [15] Krapez JC, Cielo P. Thermographic nondestructive evaluation: data inversion procedures part I: 1D analysis. *Res Nondestruct Eval* 1991;3(2):81–100.
- [16] Lam, Teng. Ultimate condition of fiber reinforced polymer-confined concrete. *ASCE J Compos Constr* 2004;8(6):539–48.
- [17] ASTM D3039/D3039M. *Standard test method for tensile properties of polymer matrix composite materials*. West Conshohocken (Pa); 1995.
- [18] Gonzalez RC, Wintz P. *Digital image processing*. 2nd ed. Reading (MA): Addison-Wesley; 1987.
- [19] Lau SK, Almond DP, Patel M, Corbett J, Quigley MBC. Analysis of transient thermal inspection. In: Lettington AH, editors. *Infrared technology and applications*, proceedings of the SPIE; 1990; 1320: 178–85.
- [20] Starnes MA, Carino NJ, Kausel EA. Preliminary thermography studies for quality control of concrete structures strengthened with fiber-reinforced polymer composites. *J Mater Civ Eng* 2003;15(3):266–73.
- [21] Bank LC, Gentry TR. Accelerated test methods to determine the long-term behaviour of FRP composite structures: environmental effects. *J Reinf Plast Compos* 1995; 14(June): 558–87.
- [22] Silva MAG, Biscaia H. Degradation of bond between FRP and RC beams. *Compos Struct* 2008;85(2):164–74.
- [23] Hayes MD, Garcia K, Verghese N, Lesko JJ. The effects of moisture on the fatigue behaviour of a glass/vinyl ester composite. In: *Fiber composites in infrastructure*, proceeding of the second international conference on fiber composite in infrastructure ICCI'98, Tucson; 1998; (1): 1–13.